A continuation of the assembly of a G-quadruplex repair complex by the FANCJ DNA helicase

Laura Campbell[1,#a], Kaitlin Lowran[1,#b], Emma Cismas[1], Colin G. Wu[1*]

[1] Department of Chemistry, Oakland University, Rochester, Michigan, United States of America

[#a] Current Address: Department of Biochemistry, University of Wisconsin-Madison, Madison, Wisconsin, United States of America

[#b] Current Address: Institute of Environmental Health Sciences, Wayne State University, Detroit, Michigan, United States of America

* Corresponding author

E-mail: colinwu@oakland.edu (CGW)

Abstract

Nucleic acid sequences that are rich in guanines can form G-quadruplex (G4) structures, which can impede DNA replication or repair. The FANCJ helicase plays a role in maintaining genomic stability by facilitating DNA replication through regions of DNA that form G4 structures. This activity has been associated with an AKKQ motif in FANCJ and it is thought that this motif retains the ability to also target 8-oxoguanine-modified G4 (8oxoG4) structures. We hypothesize that the molecular recognition of FANCJ AKKQ to 8oxoG4s is dependent upon the position of DNA damage, sequence composition, and substrate stability. We previously demonstrated that reducing the loop length between guanine tetrads increased the affinity of FANCJ AKKQ when 8-oxoguanines (8oxoGs) were located at the first and fifth positions of the G4 structure. In this work, we use fluorescence spectroscopy to measure the affinities of a FANCJ AKKQ peptide for G4s formed by $(GGGT)_4$, $(GGGTT)_4$, and $(TTAGGG)_4$. G4 conformations and thermal stability were determined via circular dichroism spectroscopy. We substituted 8oxoGs at the first (8oxo1), third (8oxo3), and fifth (8oxo5) positions of each G4 sequence and found that the most destabilized structures were $(GGGT)_4$ 8oxo1, $(GGGTT)_4$ 8oxo1, and $(TTAGGG)_4$ 8oxo5 in KCl. The most destabilized structures in NaCl were $(GGGT)_4$ 8oxo1, $(GGGTT)_4$ 8oxo5, and $(TTAGGG)_4$ 8oxo5. The binding affinities of FANCJ AKKQ differed for the distinct damage positions for $(GGGT)_4$ in KCl and for $(TTAGGG)_4$ in NaCl. These findings

suggest that FANCJ AKKQ targets G4s and 8oxoG4s in a manner dependent upon sequence composition and damage position.

Introduction

G-quadruplexes

G-quadruplexes (G4s) are stable secondary DNA structures found in guanine-rich sequences. These structures arise via intramolecular Hoogsteen hydrogen bonding reactions in single-stranded (ss) DNA that contains four stretches of three or more consecutive guanines [1]. Monovalent cations further stabilize these interactions by centrally coordinating the G4 structure. The two most biologically relevant cations are potassium and sodium, with potassium ions generally having a greater impact on stability [2-4].

The general sequence for G4s has been accepted as $(GGGN_{1\text{-}7})_4$, with N representing any DNA base(s) [5]. This has led to an estimate of over 400,000 G4 motifs being identified in the human genome [6]. Depending on solution conditions and intervening loop sequence, G4s can adopt three main spatial conformations: parallel, antiparallel, and hybrid (Fig 1) [4, 7]. These conformations are classified based on how the intervening sequence, $N_{1\text{-}7}$, links the guanine tetrads [8, 9]. Circular dichroism (CD) spectroscopy can be used to observe the optical properties of these conformations [10].

54 The respective spatial arrangements are important as certain G4-binding proteins have
55 preference or specificity for specific conformations; for example, the Pif1 helicase was
56 shown to preferentially unfold antiparallel G4s [11-15].

57 G4s are abundant in regions associated with genome regulation [5, 16, 17]. Due to
58 this accumulation, G4s are thought to play a role in translation regulation, splicing
59 modulation, and telomere capping [18- 20]. However, despite this apparent involvement,
60 an accumulation of G4s can be toxic to cells as they stall DNA repair, replication, and
61 RNA transcription [16]. The regulation of G4 formation has consequently emerged as a
62 novel therapeutic target for diseases. G4 stabilizers such as CX-5461 take advantage of
63 this fact by inducing replication fork blockage and single-stranded gaps or breaks [21].

64 An additional problem present in G4s is the susceptibility of guanine to reactive
65 oxygen species. Guanine has the lowest oxidation potential of all DNA base pairs and is
66 the most susceptible to oxidative damage from reactive oxygen species [22]. Consecutive
67 runs or stacking of guanines further lowers their oxidation potential [23]. When guanine
68 undergoes oxidative damage, it is commonly known as 8-oxoguanine (8oxoG). Due to
69 the ability of 8oxoG to pair with both adenine and cytosine, 8oxoGs can cause guanine-
70 to-thymine transversion mutations if left unrepaired [24, 25]. While 8oxoG-modified G4s
71 (8oxoG4s) can still form stable structures, the damage can cause a decrease in stability,
72 ultimately leaving the DNA vulnerable to cellular nucleases and causing untimely
73 shortening [26, 27]. It was also shown, via NMR, that the incorporation of 8oxoG into the

74 human telomeric G4 changed the G4 conformation by converting guanine glycosidic
75 angles from *anti* to *syn* conformations [26].

76 FANCJ

77 Fanconi anemia complementation group J (FANCJ) is an iron-sulfur helicase that
78 participates in the human DNA cross-link repair pathway [28]. Mutations in *FANCJ* can
79 lead to an increased risk of cancer and the development of Fanconi anemia [28-30].
80 Previous studies have shown that FANCJ coordinates the repair of DNA intermediates
81 arising from the nucleotide excision repair pathway [31-33]. Specifically, FANCJ binds to
82 G4-rich regions and supports DNA replication by unwinding G4s [31, 34]. When a
83 polymerase is stalled by G4 obstructions, FANCJ is able to bind the G4 and unfold the
84 structure [35]. FANCJ can then recruit another polymerase, such as the translesion
85 polymerase REV1, to continue with replication (Fig 2) [36].

86 An unrelated RNA helicase and G4 binding protein, RHAU, targets G4s and
87 8oxoG4s through an AKKQ motif. In this motif, the two lysine residues are readily
88 available for DNA binding [11, 37]. FANCJ has also been identified to contain a similar
89 AKKQ motif at K141/K142 [33]. This motif (Fig 3) allows FANCJ to bind and anchor to
90 G4s and 8oxoG4s [36]. In this work, we examine the interactions of FANCJ AKKQ with
91 G4s and 8oxoG4s of varying intervening sequence lengths and position of damage. These
92 interactions are related to G4 conformation and thermal stability to further characterize

93 the recognition of G4 and 8oxoG4 sequences by FANCJ AKKQ. Previous data is included
94 from our study of $(GGGT)_4$ and $(TTAGGG)_4$; we expand upon this work here by
95 introducing a third sequence, $(GGGTT)_4$, with 8oxoGs systematically substituted at the
96 first, third, and fifth guanines of each G4 sequence.

97 Results

98 G-quadruplex conformation and thermal stability

99 CD spectroscopy was used to determine the conformation and thermal stability of
100 twelve G4 sequences in KCl and NaCl solutions. G4 structures have distinct optical
101 properties that give unique CD intensity signals (Fig 4A) [9, 10]. Moreover, CD
102 spectroscopy was used to determine the melting temperature (T_m) of G4 structures [38].
103 As temperature increases, the G4 structure unfolds, and the intensity of spectral peaks
104 and troughs decreases (Fig 4B). The change in intensity can be analyzed as a function of
105 temperature to determine the T_m, which is a direct indicator of thermal stability (Fig 4C).

106 The three undamaged G4 sequences were chosen based on intervening sequence
107 length and biological relevance. $(GGGT)_4$ is an HIV-1 integrase aptamer and contains a
108 single thymine base for the loop [7, 39]. G4 sequences that contain only single-residue
109 loops are shown to adopt a compact, parallel conformation, with thymine having the
110 most stability [7, 40]. $(TTAGGG)_4$ is commonly referred to as the human telomeric

111 sequence due to its repetition at the ends of human chromosomes and its protective role
112 in maintaining telomere length [19]. $(GGGTT)_4$ is an artificial sequence designed to have
113 a loop of intermediate length.

114 An 8oxoG-modified base was substituted for the first (8oxo1), third (8oxo3), or
115 fifth (8oxo5) guanine position of each G4 sequence (Fig 5). These positions were chosen
116 as previous studies for the human telomeric sequence showed that 8oxo5 was the most
117 thermally destabilized, 8oxo1 was the least destabilized, and 8oxo3 had an intermediate
118 level of destabilization [27]. Furthermore, this places an 8oxoG in each of the three tetrads
119 of a G4 structure.

120 We previously studied the G4 conformations and melting temperatures of the
121 $(GGGT)_4$ and $(TTAGGG)_4$ sequences with oxidative damage induced at the 8oxo1 and
122 8oxo5 positions [36]. This data was performed in both KCl- and NaCl-containing buffers
123 and is included in this manuscript for reference. In this study, we introduce damage to
124 the 8oxo3 position of the $(GGGT)_4$ and $(TTAGGG)_4$ sequences and study all three
125 positions of oxidative damage in the $(GGGTT)_4$ sequence.

126 All $(GGGT)_4$ sequences formed a parallel conformation in KCl (Fig 6A). Based on
127 the overlaying CD spectra traces, 8oxoG-modified $(GGGT)_4$ sequences did not show
128 significant structural changes**.** Due to the limitation of the machine, 95 °C was the
129 maximum temperature reached. As evident in Fig 6B, $(GGGT)_4$ is not fully unfolded at 95
130 °C and the T_m can be assumed to be > 88.4 ± 8.4 °C (Table 1). This assumption is in

131 agreement with previous studies [7]. Each T_m value for the $(GGGT)_4$ 8oxoG4s showed a
132 decrease from the native sequence, with $(GGGT)_4$ 8oxo1 having the highest decrease in
133 thermal stability of ΔT_m = -19.0 ± 8.4 °C and $(GGGT)_4$ 8oxo3 having the lowest change of
134 ΔT_m = -8.1 ± 8.4 °C.

135 $(GGGTT)_4$ also formed a parallel conformation in KCl (Fig 6C). $(GGGTT)_4$ 8oxo1
136 and $(GGGTT)_4$ 8oxo5 sequences similarly formed parallel conformations, yet with slight
137 structural changes, as evident by differences in the CD spectra traces from 300 to 280 nm.
138 Conversely, the $(GGGTT)_4$ 8oxo3 sequence changed $(GGGTT)_4$ to an antiparallel
139 sequence. The T_m of $(GGGTT)_4$ was determined to be 83.5 ± 0.7 °C (Fig 6D; Table 1). Similar
140 to the $(GGGT)_4$ sequences in KCl, $(GGGTT)_4$ 8oxo1 had the highest decrease in thermal
141 stability of ΔT_m = -31.5 ± 1.6 °C while $(GGGTT)_4$ 8oxo3 had the lowest change of ΔT_m = -
142 26.3 ± 0.7 °C.

143 $(TTAGGG)_4$ formed a hybrid conformation in KCl (Fig 6E). $(TTAGGG)_4$ 8oxo1 and
144 $(TTAGGG)_4$ 8oxo5 sequences also formed hybrid conformations, although with
145 significant structural changes. $(TTAGGG)_4$ 8oxo1 had a significant right shift in the 295
146 nm peak and a double trough at 260 and 240 nm. $(TTAGGG)_4$ 8oxo5 experienced
147 depression in its peak at 295 nm and an increase in its shoulder at 260 nm and trough at
148 240 nm. Similar to $(GGGTT)_4$ 8oxo3, the $(TTAGGG)_4$ 8oxo3 sequence changed to the
149 antiparallel conformation. $(TTAGGG)_4$ had a T_m of 62.5 ± 0.5 °C (Fig 6F; Table 1).
150 Concurrent with previous literature, $(TTAGGG)_4$ 8oxo5 had the highest decrease in

151 thermal stability of ΔT_m = -23.6 ± 0.8 °C while $(TTAGGG)_4$ 8oxo1 had the lowest change in

152 thermal stability of ΔT_m = -8.0 ± 0.7 °C [27].

153 **Table 1. Summary of G4 conformation and melting temperature in 150 mM KCl**

Name	Conformation	T_m (°C)	Δ T_m (°C)
$(GGGT)_4$	Parallel	> 88.4 ± 8.4	-
$(GGGT)_4$ 8oxo1	Parallel	69.4 ± 0.6	-19.0 ± 8.4
$(GGGT)_4$ 8oxo3	Parallel	80.3 ± 0.4	-8.1 ± 8.4
$(GGGT)_4$ 8oxo5	Parallel	71.6 ± 0.4	-16.8 ± 8.4
$(GGGTT)_4$	Parallel	83.5 ± 0.7	-
$(GGGTT)_4$ 8oxo1	Parallel	52.0 ± 1.4	-31.5 ± 1.6
$(GGGTT)_4$ 8oxo3	Antiparallel	57.2 ± 0.3	-26.3 ± 0.7
$(GGGTT)_4$ 8oxo5	Parallel	55.9 ± 0.3	-27.6 ± 0.8
$(TTAGGG)_4$	Hybrid	62.5 ± 0.5	-
$(TTAGGG)_4$ 8oxo1	Hybrid-esque	54.5 ± 0.5	-8.0 ± 0.7
$(TTAGGG)_4$ 8oxo3	Antiparallel	49.5 ± 0.3	-13.0 ± 0.6
$(TTAGGG)_4$ 8oxo5	Hybrid-esque	38.9 ± 0.6	-23.6 ± 0.8

154

155 As in KCl, all $(GGGT)_4$ sequences formed parallel conformations in NaCl (Fig 7A).

156 However, all three $(GGGT)_4$ 8oxoG4 sequences experienced a slight change in structure,

157 as indicated by the differences in traces in the 300 to 280 nm region. $(GGGT)_4$ was
158 determined to have a T_m of 70.3 ± 0.7 °C (Fig 7B; Table 2). Similar to $(GGGT)_4$ in KCl,
159 $(GGGT)_4$ 8oxo1 had the highest decrease in thermal stability of ΔT_m = -27.8 ± 0.9 °C while
160 $(GGGT)_4$ 8oxo3 had the lowest change of ΔT_m = -13.9 ± 0.8 °C.

161 The native $(GGGTT)_4$ also formed a parallel conformation in NaCl (Fig 7C).
162 However, all $(GGGTT)_4$ 8oxoG4 sequences experienced a conformational change.
163 $(GGGTT)_4$ 8oxo1 and $(GGGTT)_4$ 8oxo3 formed antiparallel conformations, while
164 $(GGGTT)_4$ 8oxo5 formed a hybrid conformation. $(GGGTT)_4$ had a T_m of 44.8 ± 1.2 °C (Fig
165 7D; Table 2). $(GGGTT)_4$ 8oxo1 and $(GGGTT)_4$ 8oxo3 did not show a significant change in
166 thermal stability, with $(GGGTT)_4$ 8oxo1 even having an increase of ΔT_m = 2.4 ± 1.2 °C.
167 $(GGGTT)_4$ 8oxo5 had a significant change of ΔT_m = -17.3 ± 1.4 °C. The $(GGGTT)_4$ 8oxo5
168 thermal melt was taken over -5 to 75 °C because it did not appear fully folded at 15 °C.

169 $(TTAGGG)_4$ and its 8oxoG4 sequences formed antiparallel conformations in NaCl
170 (Fig 7E). All $(TTAGGG)_4$ 8oxoG4 sequences showed slight differences in intensities and
171 peak shifts from the spectra of the native sequence, indicating slight structural
172 differences. The T_m of $(TTAGGG)_4$ was determined to be 52.1 ± 0.3 °C (Fig 7F; Table 2).
173 Concurrent with previous literature and the KCl data above, $(TTAGGG)_4$ 8oxo5 had the
174 highest decrease in thermal stability of ΔT_m = -18.8 ± 0.5 °C while $(TTAGGG)_4$ 8oxo1 had
175 the lowest of ΔT_m = -4.3 ± 0.7 °C [27].

176 **Table 2. Summary of G4 conformation and melting temperature in 150 mM NaCl**

Name	Conformation	T_m (°C)	Δ T_m (°C)
$(GGGT)_4$	Parallel	70.3 ± 0.7	-
$(GGGT)_4$ 8oxo1	Parallel	42.5 ± 0.5	-27.8 ± 0.9
$(GGGT)_4$ 8oxo3	Parallel	56.4 ± 0.4	-13.9 ± 0.8
$(GGGT)_4$ 8oxo5	Parallel	44.0 ± 0.3	-26.3 ± 0.8
$(GGGTT)_4$	Parallel	44.8 ± 1.2	-
$(GGGTT)_4$ 8oxo1	Antiparallel	47.2 ± 0.3	2.4 ± 1.2
$(GGGTT)_4$ 8oxo3	Antiparallel	44.6 ± 0.2	-0.2 ± 1.2
$(GGGTT)_4$ 8oxo5	Hybrid-esque	27.5 ± 0.9	-17.3 ± 1.4
$(TTAGGG)_4$	Antiparallel	52.1 ± 0.3	-
$(TTAGGG)_4$ 8oxo1	Antiparallel	47.8 ± 0.6	-4.3 ± 0.7
$(TTAGGG)_4$ 8oxo3	Antiparallel	42.2 ± 0.7	-9.9 ± 0.8
$(TTAGGG)_4$ 8oxo5	Antiparallel	33.3 ± 0.4	-18.8 ± 0.5

FANCJ AKKQ binding

Fluorescence spectroscopy titrations were used to determine the interaction strength between AKKQ and G4 sequences. The AKKQ sequence examined was modified to contain a tryptophan residue, W, at the C-terminal end of the sequence (Fig 8A). Due to its aromatic properties, tryptophan produces a fluorescence peak from 300 to

183 450 nm. When bound to DNA, this signal is quenched, and the binding strength can be
184 determined by the decrease in fluorescence intensity (Fig 8B). This decrease in the
185 integrated peak was plotted against increasing DNA concentration, and the resulting
186 curve fit to a 1:1 equilibrium binding interaction model using a nonlinear least squared
187 analysis (Fig 8C). The resulting K value represents an equilibrium K for forming the
188 protein-DNA complex.

189 Previously, we demonstrated that shortening the intervening loop length
190 increased the affinity of FANCJ AKKQ when 8oxoGs were located at the 8oxo1 and 8oxo5
191 positions of the G4 structure [36]; however, our study was limited to the $(GGGT)_4$ and
192 $(TTAGGG)_4$ sequences in KCl-containing buffer. We include this previous data for
193 comparison. In this study, we additionally study the $(GGGT)_4$ sequence with oxidative
194 damage induced at the 8oxo1, 8oxo3, and 8oxo5 positions of all three G4 sequences. We
195 also perform these binding analyses in NaCl-containing buffer.

196 Binding interactions between FANCJ AKKQ and the G4 sequences were first
197 analyzed in buffer containing 150 mM KCl (Fig 9). Binding affinities are summarized in
198 Table 3. For the $(GGGT)_4$ sequences, AKKQ had the strongest interaction with $(GGGT)_4$
199 8oxo1 ($K = 7.7 \pm 0.7 \times 10^5\ M^{-1}$), followed by $(GGGT)_4$ 8oxo5 ($K = 4.4 \pm 0.6 \times 10^5\ M^{-1}$), then
200 $(GGGT)_4$ 8oxo3 ($K = 3.2 \pm 0.1 \times 10^5\ M^{-1}$), and lastly the undamaged native sequence (K =
201 $2.7 \pm 0.4 \times 10^5\ M^{-1}$). AKKQ bound strongest to the native $(GGGTT)_4$ sequence ($K = 6.0 \pm 0.9$
202 $\times 10^5\ M^{-1}$) and weakest to the respective $(GGGTT)_4$ 8oxoG4s ($K = 8\text{-}9 \times 10^5\ M^{-1}$). No

203 significant changes in interaction were observed between the 8oxo1, 8oxo3, and 8oxo5
204 damage positions for the $(GGGTT)_4$ sequence. AKKQ displayed no preference for the
205 8oxoG4 damage positions of $(TTAGGG)_4$ and bound with similar affinity to the native
206 sequence. Each K value for the $(TTAGGG)_4$ sequences was within error of 1.3-1.4 x 10^6 M^{-}
207 ^{1}.

208 **Table 3. Summary of FANCJ AKKQ-G4 binding by fluorescence spectroscopy in 150**
209 **mM KCl**

Name	K (M^{-1})	R^2
$(GGGT)_4$	2.7 ± 0.4 x 10^5	0.997
$(GGGT)_4$ 8oxo1	7.7 ± 0.7 x 10^5	0.998
$(GGGT)_4$ 8oxo3	3.2 ± 0.1 x 10^5	0.997
$(GGGT)_4$ 8oxo5	4.4 ± 0.6 x 10^5	0.997
$(GGGTT)_4$	6.0 ± 0.9 x 10^5	0.997
$(GGGTT)_4$ 8oxo1	8.2 ± 1.0 x 10^5	0.997
$(GGGTT)_4$ 8oxo3	9.6 ± 1.0 x 10^5	0.996
$(GGGTT)_4$ 8oxo5	9.3 ± 0.8 x 10^5	0.997
$(TTAGGG)_4$	1.6 ± 0.7 x 10^6	0.996
$(TTAGGG)_4$ 8oxo1	1.3 ± 0.4 x 10^6	0.997
$(TTAGGG)_4$ 8oxo3	1.2 ± 0.1 x 10^6	0.996

$(TTAGGG)_4$ 8oxo5	$1.4 \pm 0.5 \times 10^6$	0.997

These binding experiments were repeated in buffer containing 150 mM NaCl (Fig 10). Binding affinities are summarized in Table 4. As in KCl, FANCJ AKKQ showed a preference for specific 8oxoG damage positions in the $(GGGT)_4$ sequences. AKKQ bound strongest to $(GGGT)_4$ 8oxo5 and $(GGGT)_4$ 8oxo1 (K= $3.4 \pm 0.5 \times 10^5$ M^{-1} for both), followed by $(GGGT)_4$ 8oxo3 (K = $2.9 \pm 0.5 \times 10^5$ M^{-1}), and lastly the native sequence (K = $2.3 \pm 0.3 \times 10^5$ M^{-1}). AKKQ bound with similar affinity to the native $(GGGTT)_4$ sequence, $(GGGTT)_4$ 8oxo5, and $(GGGTT)_4$ 8oxo3 (K = $4.9\text{-}5.6 \times 10^5$ M^{-1}), with the weakest affinity for $(GGGTT)_4$ 8oxo1 (K = $3.9 \pm 1.3 \times 10^5$ M^{-1}). For the $(TTAGGG)_4$ sequences, AKKQ bound strongest to $(TTAGGG)_4$ 8oxo5 (K = $1.5 \pm 0.1 \times 10^6$ M^{-1}), followed by the native sequence and $(TTAGGG)_4$ 8oxo1 (K = 6.5×10^5 M^{-5} for both), and lastly $(TTAGGG)_4$ 8oxo3 (K = $5.1 \pm 1.1 \times 10^5$ M^{-1}).

Table 4. Summary of FANCJ AKKQ-G4 binding by fluorescence spectroscopy in 150 mM NaCl

Name	K (M^{-1})	R^2
$(GGGT)_4$	$2.3 \pm 0.3 \times 10^5$	0.9997
$(GGGT)_4$ 8oxo1	$3.4 \pm 0.5 \times 10^5$	0.9996
$(GGGT)_4$ 8oxo3	$2.9 \pm 0.5 \times 10^5$	0.9994
$(GGGT)_4$ 8oxo5	$3.4 \pm 0.5 \times 10^5$	0.9997

$(GGGTT)_4$	$4.9 \pm 2.0 \times 10^5$	0.9995
$(GGGTT)_4$ 8oxo1	$3.9 \pm 1.3 \times 10^5$	0.9993
$(GGGTT)_4$ 8oxo3	$5.2 \pm 1.7 \times 10^5$	0.9994
$(GGGTT)_4$ 8oxo5	$5.6 \pm 1.1 \times 10^5$	0.9992
$(TTAGGG)_4$	$6.5 \pm 0.6 \times 10^5$	0.9991
$(TTAGGG)_4$ 8oxo1	$6.5 \pm 1.4 \times 10^5$	0.9996
$(TTAGGG)_4$ 8oxo3	$5.1 \pm 1.1 \times 10^5$	0.9998
$(TTAGGG)_4$ 8oxo5	$1.1 \pm 0.1 \times 10^6$	0.9974

Discussion

G-quadruplexes

The CD data for the human telomeric sequence is concurrent with previous studies in that $(TTAGGG)_4$ and its respective 8oxoG4 sequences form hybrid and antiparallel conformations in KCl and antiparallel conformations in NaCl [26, 27, 41]. In both KCl and NaCl, the $(TTAGGG)_4$ 8oxo5 sequence showed the most thermal instability, while $(TTAGGG)_4$ 8oxo1 showed the least [27]. This pattern was also observed with the $(GGGTT)_4$ 8oxoG-modified sequences in NaCl. While $(GGGTT)_4$ formed a parallel conformation, its 8oxoG4 analogs formed antiparallel or hybrid conformations. Conversely, a different pattern of stability was observed in the other substrates. $(GGGT)_4$

233 sequences in KCl and NaCl and $(GGGTT)_4$ sequences in KCl formed predominately
234 parallel conformations, with only $(GGGTT)_4$ 8oxo3 forming an antiparallel conformation.
235 Of these sequences, the 8oxo1 analogs had the most thermal instability, while the 8oxo3
236 analogs had the least.

237 Our results indicate that the effect of an 8oxoG on G4 thermal stability is
238 dependent upon the location of damage and the G4 structure. Sequences forming
239 compact parallel conformations were most destabilized by damage to the first guanine,
240 which resides in the bottom tetrad of the G4 structure, and were least destabilized by
241 damage to the third guanine, which resides in the top tetrad. Sequences forming the more
242 flexible antiparallel or hybrid conformations were most destabilized by damage to the
243 fifth guanine, which resides in the middle tetrad, and were least destabilized by damage
244 to the first guanine. A similar destabilizing effect had already been observed in the hybrid
245 conformation of the human telomeric G4 sequence when an 8oxoG was substituted at the
246 fifth guanine position [26].

247 Potassium and sodium ions are the most physiologically relevant monovalent
248 cations and are commonly studied in relation to G4 conformation and stability. While the
249 $(GGGT)_4$ sequences formed parallel conformations in both KCl and NaCl, most $(GGGTT)_4$
250 and $(TTAGGG)_4$ sequences folded into other conformations. The thermal stability for all
251 sequences was lower in NaCl than in KCl, suggesting that sodium ions are less effective
252 in stabilizing G4 structures. With only sodium ions present, G4 sequences cannot adopt

253 the rigid conformations that occur in the presence of potassium ions and thus form less
254 stable conformations. These findings support previous studies, suggesting that while
255 both ions can stabilize G4s, potassium ions are better suited due to their optimal size and
256 ionic strength [42].

257 It is of note that in KCl, there was a correlation between the length of the
258 intervening sequence and the thermal stability of the native sequences. $(GGGT)_4$ had the
259 highest melting temperature while $(TTAGGG)_4$ had the lowest. This indicates that as
260 intervening sequence length increases, thermal stability decreases. This observation was
261 present yet less evident in NaCl. Although $(GGGT)_4$ maintained the highest melting
262 temperature, $(GGGTT)_4$ had the lowest. These observations are in agreement with
263 previous studies [4, 40].

264 FANCJ AKKQ and G-quadruplex binding

265 Our results indicate that FANCJ AKKQ has the ability to target both G4s and
266 8oxoG4s; however, this recognition depends on the sequence composition and position
267 of damage. For the $(GGGT)_4$ sequences, which formed compact parallel conformations,
268 AKKQ bound strongest to the 8oxoG4 sequences rather than the native sequence. The
269 observed increase in binding affinity across the 8oxoG damage positions correlates with
270 a decrease in thermal stability. $(GGGT)_4$ 8oxo1 had the greatest decrease in thermal
271 stability and the strongest interaction with AKKQ. Conversely, $(GGGT)_4$ 8oxo3 had the

272 lowest decrease in thermal stability and the weakest interaction with AKKQ. As the CD
273 spectra displayed no change in structural stability (Fig 6A), this implies that AKKQ is
274 targeting the 8oxoG position rather than the intervening loop.

275 For the $(GGGTT)_4$ sequences, which formed predominantly parallel
276 conformations, AKKQ preferentially bound to the 8oxoG4 sequences with no significant
277 changes in affinity between each damage position. Assuming that AKKQ is targeting the
278 intervening sequence, the preference for the 8oxoG4s can be attributed to the
279 destabilization of the G4 structure. Though $(GGGTT)_4$ 8oxo1 and 8oxo5 still formed
280 parallel conformations, the CD spectra indicated destabilization in the 280 to 300 nm
281 range (Fig 6C). This destabilization may have led to the intervening sequence being more
282 exposed than in an undamaged parallel conformation, thus facilitating better access for
283 AKKQ.

284 AKKQ bound with similar affinity to all $(TTAGGG)_4$ sequences, which form the
285 less rigid hybrid or antiparallel conformations and thus expose the DNA loop. This
286 implies that AKKQ preferentially targets the intervening sequence and is not affected by
287 oxidative damage in $(TTAGGG)_4$. It is of note that in KCl, FANCJ AKKQ bound to the
288 $(TTAGGG)_4$ sequences with an order of magnitude higher than the other G4 sequences.
289 However, upon changing the salt to NaCl, AKKQ bound equally to all sequences except
290 for the $(TTAGGG)_4$ 8oxo5 sequence, to which it bound an order of magnitude stronger.

291 One possible explanation for the observed differences in binding preferences is
292 that high sodium concentrations affect the electrostatic interactions between the peptide
293 and the G4s. Sodium ions are known to provide less stabilization to G4s compared to
294 potassium [2-4]. We anticipated the FANCJ AKKQ peptide to adopt an alpha helical
295 structure due to previous NMR studies of the structurally and sequentially similar AKKQ
296 motif of the G4-binding protein RHAU [11]. Although our CD studies (Supporting
297 information) did not detect any alpha helical structure in either salt, the addition of
298 trifluoroethanol revealed a helical-like structure in both salt conditions. However, the
299 spectra obtained in each salt were not superimposable. This suggests that sodium ions
300 stabilize the peptide to a different extent than potassium ions.

301 As FANCJ is a DNA repair helicase, it was anticipated that FANCJ AKKQ would
302 bind preferentially to 8oxoGs to facilitate their repair. However, a preference for the
303 8oxoG4 sequences was only observed for the $(GGGT)_4$ sequences, suggesting that FANCJ
304 AKKQ may instead target the intervening sequence. This is further supported by the
305 positive correlation between binding interaction and intervening sequence length in the
306 undamaged G4 structures. A proposed interaction model for AKKQ and 8oxoG4s is
307 illustrated in Fig 11.

308 Previous work has demonstrated that FANCJ collaborates with the translesion
309 polymerase REV1, which unwinds G4 structures, for the successful replication of G4-rich
310 DNA strands [43]. It is possible that FANCJ and REV1 are responsible for repairing

311 distinct types of G4 DNA. FANCJ appears to prefer G4 structures with exposed loops,
312 while REV1 may prefer more compact G4 structures. Future work should aim to
313 characterize the interaction of REV1 with G4s and 8oxoG4s. Furthermore, G4 damage
314 positions were limited to the first, third, and fifth guanine in this study; it should be
315 observed whether the trends identified in this study persist with systematic substitution
316 of 8oxoGs for each G4 damage position.

317 Materials and Methods

318 Buffers and reagents

319 All buffers and reagents were prepared with reagent-grade chemicals and Type I
320 water purified with a Smart2Pure 6 UV/UF system (ThermoFisher, Waltham, MA).
321 Solutions were sterilized through a 0.22 μm PES filter.

322 Peptide and DNA oligos

323 FANCJ AKKQ peptide (129-PEKTTLAAKLSAKKQASIW-147) was synthesized
324 by Genscript (Piscataway, NJ), and the powder was dissolved into 20 mM HEPES pH 7.5,
325 150 mM KCl or NaCl, 5 mM TCEP, and 5% (v/v) glycerol. Protein concentration was
326 determined using a NanoDrop One UV-Vis microvolume spectrophotometer
327 (ThermoFisher) and the molar extinction coefficients below. Peptide samples were
328 aliquoted, frozen, and stored at -20 °C. Oligodeoxyribonucleotides were purchased from

329 Integrated DNA Technologies (IDT, Coralville, IA) and concentrations were determined
330 similarly to the above stated. DNA substrates were stored at 4 °C. A list of sequences used
331 is described in Table 5.

332 **Table 5. DNA Sequences.**

Name	Sequence (5′→3′)	Molar Extinction Coefficient ($M^{-1}cm^{-1}$)	Molecular Weight (g/mol)
$(GGGT)_4$	GGGTGGGTGGGTGGGT	157200	5105.3
$(GGGT)_4$ 8oxo1	T/i8oxodG/GGTGGGTGGGTGGGT	159100	5425.5
$(GGGT)_4$ 8oxo3	GG/i8oxodG/TGGGTGGGTGGGT	151600	5121.3
$(GGGT)_4$ 8oxo5	GGGTG/i8oxodG/GTGGGTGGGT	151600	5121.3
$(GGGTT)_4$	GGGTTGGGTTGGGTTGGGTT	189600	6322.1
$(GGGTT)_4$ 8oxo1	/i8oxodG/GGTTGGGTTGGGTTGGGTT	184000	6338.1

$(GGGTT)_4$ 8oxo3	GG/i8oxodG/TTGGGTGGGTTGGGTT	184000	6338.1
$(GGGTT)_4$ 8oxo5	GGGTTG/i8oxodG/GTTGGGTTGGGTT	184000	6338.1
$(TTAGGG)_4$	TTAGGGTTAGGGTTAGGGTTAGGG	244600	7575.0
$(TTAGGG)_4$ 8oxo1	TTA/i8oxodG/GGTTAGGGTTAGGGTTA GGG	239000	7590.9
$(TTAGGG)_4$ 8oxo3	TTAGG/i8oxodG/TTAGGGTTAGGGTTA GGG	239000	7590.9
$(TTAGGG)_4$ 8oxo5	TTAGGGTTAG/i8oxodG/GTTAGGGTTA GGG	239000	7590.9

CD spectroscopy

CD measurements were performed on a JASCO J-810 spectropolarimeter equipped with a PTC-423S peltier system and Koolance Liquid Cooling System. G4 DNA samples were dialyzed into 20 mM boric acid, 150 mM KCl or NaCl. CD spectra scans were taken from 220 nm to 320 nm at 25 °C with DNA samples of 0.3 mg/mL. Five traces for each DNA sample were taken and averaged. A reference scan of buffer alone was subtracted from the averaged scan. Temperature melt scans were taken from 15 °C to 95 °C at 262 nm (for parallel conformations) or 295 nm (for antiparallel and hybrid

341 conformation). Samples were heated to 95 °C and allowed to cool overnight prior to the
342 first melt. Three trials for each DNA sample were taken and averaged.

343 Melting temperature was determined using SigmaPlot as an analysis program and
344 the model described below by Greenfield for a two-state transition of a monomer from a
345 folded to an unfolded state [44]. This analysis is based on the Gibbs-Helmholtz equation
346 where ΔG represents Gibbs free energy, ΔH represents enthalpy, ΔC_P represents the
347 change in heat capacity, K represents the folding constant, and y represents the fraction
348 of folded DNA at any given temperature, T. θ_t is the observed ellipticity at any
349 temperature, θ_F is the observed ellipticity of the folded DNA, and θ_U is the observed
350 ellipticity of the unfolded DNA. The melting temperature, T_m, of the DNA can then be
351 calculated as the temperature where y = 0.5.

352 $$\Delta G = \Delta H\left(1 - \frac{T}{T_m}\right) - \Delta C_p((T_m - T) + T\left(\ln\left(\frac{T}{T_m}\right)\right))$$

353 $$K = e^{(-\frac{\Delta G}{RT})}$$

354 $$y = \frac{K}{1 + K}$$

355 $$[\theta]_t = \left(([\theta]_F - [\theta]_U) * y\right) + [\theta]_U$$

356 ## Fluorescence spectroscopy

357 Fluorescence spectroscopy measurements were performed on a Cary Eclipse
358 Fluorescence Spectrophotometer (Agilent Technologies, Santa Clara, CA) equipped with

359 a PCB 1500 water peltier system. Spectra were taken from 300 nm to 450 nm with the
360 excitation at 280 nm and temperature at 25 °C. A scan of buffer alone, 20 mM HEPES pH
361 7.5, 150 mM KCl or NaCl, 5 mM TCEP, and 5% (v/v) glycerol, was used as a baseline.
362 FANCJ AKKQ peptide (5 μM) was titrated with additions of a DNA substrate. The
363 mixture was allowed to equilibrate for 3 minutes before taking each spectra scan.

364 Observed fluorescence quenching (ΔF) was calculated using the following
365 equation, with F_0 representing total fluorescence from the FANCJ peptide alone and F_i
366 representing the total fluorescence after the *i*th addition of DNA:

367 $$\Delta F = \frac{F_0 - F_i}{F_0}$$

368 Binding isotherms were calculated by plotting ΔF versus total DNA concentration.
369 The resulting curve was fit to a 1:1 interaction model using Scientist 2.0 software
370 (Micromath, St. Louis, MO) to calculate an equilibrium K. The equilibrium K was
371 calculated using the following formulas, where A was the amplitude of fluorescence
372 quenching and K was the equilibrium association constant. D_f and D_t were the free and
373 total concentration of DNA, while P_f and P_t described the free and total peptide
374 concentration. Fluorescence titrations were performed in triplicate. The reported K values
375 were determined from an average of three independent data-sets.

$$\Delta F_{obs} = A\left(\frac{KD_f}{1+KD_f}\right)$$
$$D_t = D_f(1+KP_f)$$
$$P_t = P_f(1+KD_f)$$

Acknowledgements

Figs 1, 3-5, 8A, and 11 were created with BioRender.com.

Author contributions

CGW designed experiments. LC, KL, and CGW acquired data and interpreted results. LC, KL, EC, and CGW prepared the manuscript draft. All authors have read and agreed to the published version of the manuscript.

Financial disclosure statement

This work was supported by NSF grant 2142839 and AHA grant 19AIREA34460026 to CGW.

Competing interests

Authors have no conflict of interest to disclose.

References

1. Bochman ML, Paeschke K, Zakian VA. DNA secondary structures: stability and function of G-quadruplex structures. Nature Reviews Genetics. 2012;13(11):770-80.
2. Nový J, Böhm S, Králová J, Král V, Urbanová M. Formation and temperature stability of G-quadruplex structures studied by electronic and vibrational circular dichroism spectroscopy combined with ab initio calculations. Biopolymers. 2008;89(2):144-52.
3. Chaires JB. Human telomeric G-quadruplex: thermodynamic and kinetic studies of telomeric quadruplex stability. The FEBS Journal. 2010;277(5):1098-106.
4. Guédin A, Gros J, Alberti P, Mergny J-L. How long is too long? Effects of loop size on G-quadruplex stability Nucleic Acids Research. 2010;38(21):7858-68.
5. Huppert JL, Balasubramanian S. Prevalence of quadruplexes in the human genome. Nucleic Acids Research. 2005;33(9):2908-16.
6. Lombardi EP, Holmes A, Verga D, Teulade-Fichou M-P, Nicolas A, Londoño-Vallejo A. Thermodynamically stable and genetically unstable G-quadruplexes are depleted in genomes across species Nucleic Acids Research. 2019;47(12):6098-113.

405 7. Hazel P, Huppert J, Balasubramanian S, Neidle S. Loop-length-dependent folding
406 of G-quadruplexes. Journal of the American Chemical Society. 2004;126(50):16405-
407 15.
408 8. Hao F, Ma Y, Guan Y. Effects of Central Loop Length and Metal Ions on the
409 Thermal Stability of G-Quadruplexes. Molecules. 2019;24(10).
410 9. Burge S, Parkinson GN, Hazel P, Todd AK, Neidle S. Quadruplex DNA:
411 sequence, topology and structure. Nucleic Acids Research. 2006;34(19):5402-15.
412 10. Villar-Guerra RD, Trent JO, Chaires JB. G-Quadruplex Secondary Structure
413 Obtained from Circular Dichroism Spectroscopy. Angewandte Chemie.
414 2018;57(24):7171-5.
415 11. Heddi B, Cheong VV, Martadinata H, Phan AT. Insights into G-quadruplex
416 specific recognition by the DEAH-box helicase RHAU: Solution structure of a
417 peptide–quadruplex complex. Proceedings of the National Academy of Sciences
418 of the United States of America. 2015;112(31):9608-13.
419 12. Budhathoki JB, Maleki P, Roy WA, Janscak P, Yodh JG, Balci H. A Comparative
420 Study of G-Quadruplex Unfolding and DNA Reeling Activities of Human RECQ5
421 Helicase. Biophysical Journal. 2016;110(12):2585-96.
422 13. Tippana R, Hwang H, Opresko PL, Bohr VA, Myong S. Single-molecule imaging
423 reveals a common mechanism shared by G-quadruplex–resolving helicases.

424 Proceedings of the National Academy of Sciences of the United States of America.
425 2016;113(30):8448-53.
426 14. Zheng K-W, Zhang J-Y, He Y-d, Gong J-Y, Wen C-J, Chen J-N, et al. Detection of
427 genomic G-quadruplexes in living cells using a small artificial protein. Nucleic
428 Acids Research. 2020;48(20):11706-20.
429 15. Wang L, Wang Q-M, Wang Y-R, Xi X-G, Hou X-M. DNA-unwinding activity of
430 Saccharomyces cerevisiae Pif1 is modulated by thermal stability, folding
431 conformation, and loop lengths of G-quadruplex DNA. Journal of Biological
432 Chemistry. 2018;293(48):18504-13.
433 16. Rhodes D, Lipps HJ. G-quadruplexes and their regulatory roles in biology Nucleic
434 Acids Research. 2015;43(18):8627-37.
435 17. Huppert JL, Balasubramanian S. G-quadruplexes in promoters throughout the
436 human genome. Nucleic Acids Research. 2006;35(2):406-13.
437 18. Beaudoin J-D, Perreault J-P. 5'-UTR G-quadruplex structures acting as
438 translational repressors. Nucleic Acids Research. 2010;38(20):7022-36.
439 19. Smith JS, Chen Q, Yatsunyk LA, Nicoludis JM, Garcia MS, Kranaster R, et al.
440 Rudimentary G-quadruplex-based telomere capping in Saccharomyces cerevisiae.
441 Nature Structural & Molecular Biology. 2011;18(4):478-85.

442 20. Georgakopoulos-Soares I, Parada GE, Wong HY, Medhi R, Furlan G, Munita R, et
443 al. Alternative splicing modulation by G-quadruplexes. Nature Communications.
444 2022;13(1).
445 21. Xu H, Di Antonio M, McKinney S, Mathew V, Ho B, O'Neil NJ, et al. CX-5461 is a
446 DNA G-quadruplex stabilizer with selective lethality in BRCA1/2 deficient
447 tumours. Nature Communications. 2017;8.
448 22. Steenken S, Jovanovic S. How Easily Oxidizable Is DNA? One-Electron Reduction
449 Potentials of Adenosine and Guanosine Radicals in Aqueous Solution. Journal of
450 the American Chemical Society. 1997;119(3):617-8.
451 23. Oikawa S. Sequence-specific DNA damage by reactive oxygen species:
452 Implications for carcinogenesis and aging. Environmental Health and Preventive
453 Medicine. 2005;10(2):65-71.
454 24. Neeley WL, Essigmann JM. Mechanisms of Formation, Genotoxicity, and
455 Mutation of Guanine Oxidation Products. Chemical Research in Toxicology.
456 2006;19(4):491-505.
457 25. Ohno M, Sakumi K, Fukumura R, Furuichi M, Iwasaki Y, Hokama M, et al. 8-
458 oxoguanine causes spontaneous de novo germline mutations in mice. Scientific
459 Reports. 2014;4.

460 26. Bielskutė S, Plavec J, Podbevšek P. Impact of Oxidative Lesions on the Human
461 Telomeric G-Quadruplex. Journal of the American Chemical Society.
462 2019;141(6):2594-603.
463 27. Vorlícková M, Tomasko M, Sagi AJ, Bednarova K, Sagi J. 8-oxoguanine in a
464 quadruplex of the human telomere DNA sequence. The FEBS Journal.
465 2012;279(1):29-39.
466 28. Jr RMB, Cantor SB. Molecular and cellular functions of the FANCJ DNA helicase
467 defective in cancer and in Fanconi anemia. Frontiers in Genetics. 2014;5.
468 29. Palovcak A, Liu W, Yuan F, Zhang Y. Maintenance of genome stability by Fanconi
469 anemia proteins. Cell & Bioscience. 2017;7.
470 30. Datta A, Robert M. Brosh J. Holding All the Cards—How Fanconi Anemia Proteins
471 Deal with Replication Stress and Preserve Genomic Stability. Genes. 2019;10(2).
472 31. Wu Y, Shin-ya K, Jr RMB. FANCJ helicase defective in Fanconia anemia and breast
473 cancer unwinds G-quadruplex DNA to defend genomic stability. Molecular and
474 Cellular Biology. 2008;28(12):4116-28.
475 32. Cantor SB, Xie J. Assessing the link between BACH1/FANCJ and MLH1 in DNA
476 crosslink repair. Environmental and Molecular Mutagenesis. 2010;51(6):500-7.
477 33. Sarkies P, Murat P, Phillips LG, Patel KJ, Balasubramanian S, Sale JE. FANCJ
478 coordinates two pathways that maintain epigenetic stability at G-quadruplex
479 DNA. Nucleic Acids Research. 2012;40(4):1485-98.

480 34. Bosch PC, Segura-Bayona S, Koole W, Heteren JTv, Dewar JM, Tijsterman M, et al.
481 FANCJ promotes DNA synthesis through G-quadruplex structures. The EMBO
482 Journal. 2014;33(21):2521-33.
483 35. Wu CG, Spies M. G-quadruplex recognition and remodeling by the FANCJ
484 helicase. Nucleic Acids Research. 2016;44(18):8742-53.
485 36. Lowran K, Campbell L, Popp P, Wu CG. Assembly of a G-Quadruplex Repair
486 Complex by the FANCJ DNA Helicase and the REV1 Polymerase. Genes.
487 2019;11(1).
488 37. Lattmann S, Giri B, Vaughn JP, Akman SA, Nagamine Y. Role of the amino
489 terminal RHAU-specific motif in the recognition and resolution of guanine
490 quadruplex-RNA by the DEAH-box RNA helicase RHAU. Nucleic Acids
491 Research. 2010;38(18):6219-33.
492 38. Rachwal PA, Fox KR. Quadruplex melting. Methods. 2007;43(4):291-301.
493 39. Do NQ, Lim KW, Teo MH, Heddi B, Phan AT. Stacking of G-quadruplexes: NMR
494 structure of a G-rich oligonucleotide with potential anti-HIV and anticancer
495 activity. Nucleic Acids Research. 2011;39(21):9448-57.
496 40. Guédin A, Cian AD, Gros J, Lacroix L, Mergny J-L. Sequence effects in single-base
497 loops for quadruplexes. Biochimie. 2008;90(5):686-96.
498 41. Lin C, Yang D. Human Telomeric G-Quadruplex Structures and G-Quadruplex-
499 Interactive Compounds. Methods in Molecular Biology. 2018:171-96.

500 42. Hardin CC, Watson T, Corregan M, Bailey C. Cation-dependent transition
501 between the quadruplex and Watson-Crick hairpin forms of d(CGCG3GCG).
502 Biochemistry. 1992;31(3):833–41.
503 43. Eddy S, Ketkar A, Zafar MK, Maddukuri L, Choi J-Y, Eoff RL. Human Rev1
504 polymerase disrupts G-quadruplex DNA. Nucleic Acids Research.
505 2014;42(5):3272-85.
506 44. Greenfield NJ. Using circular dichroism collected as a function of temperature to
507 determine the thermodynamics of protein unfolding and binding interactions.
508 Nature Protocols. 2006;1(6):2527-35.

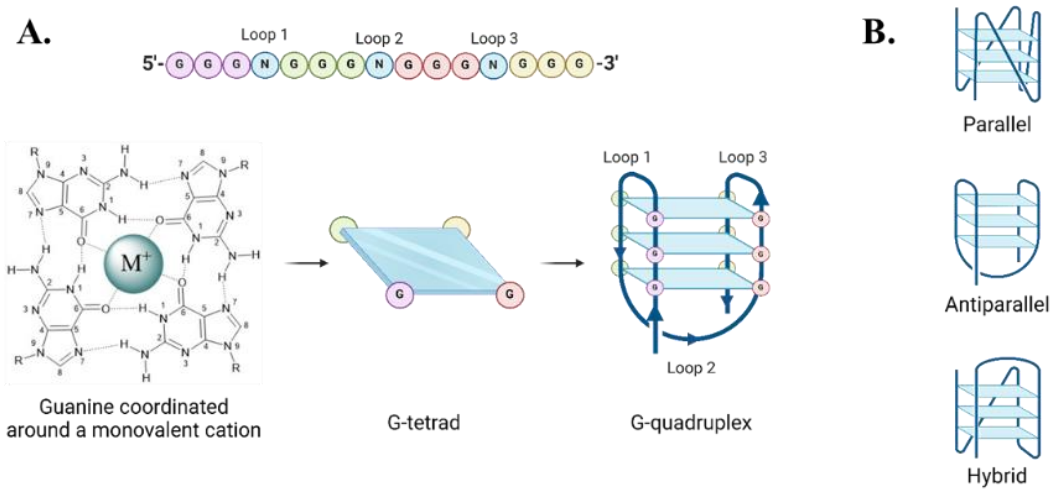

Fig 1. G-quadruplex formation and conformations.

(A) Formation of a G4 structure. (B) Graphic representation of three different intra-strand G4 conformations.

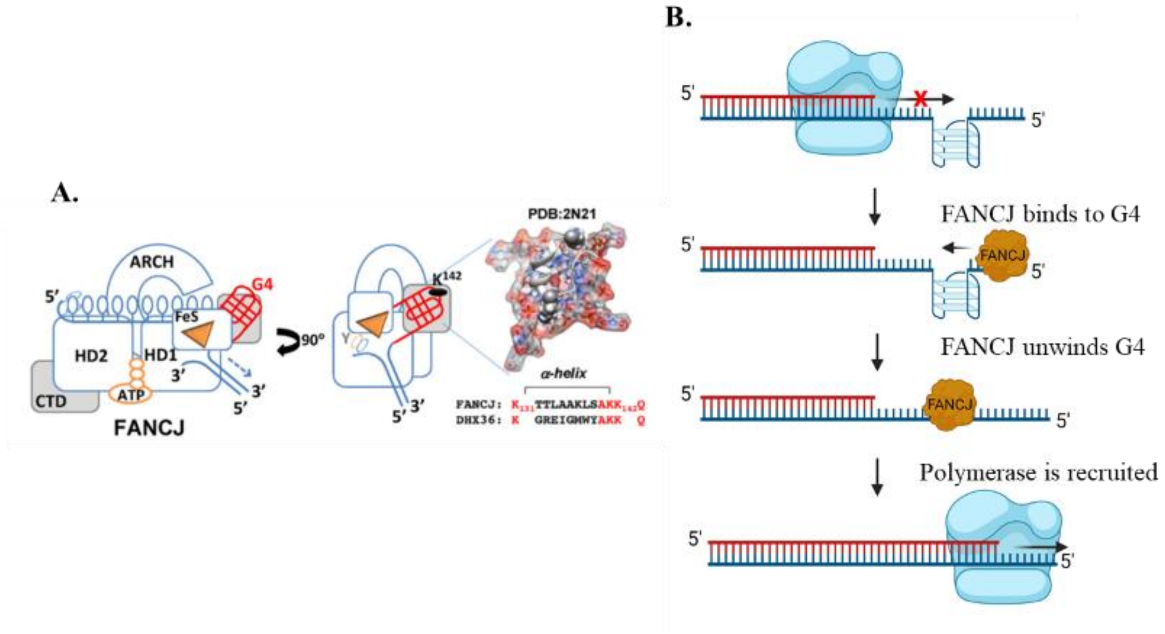

Fig 2. Molecular models of FANCJ.

(A) FANCJ possesses a G4 recognition site capable of binding G4s, and an AKKQ motif similar in structure and sequence to the AKKQ binding motif found in G4-binding protein RHAU [11, 37]. (B) The current model for FANCJ-supported DNA replication in G4-rich sequences. Upon reaching a G4 structure, the DNA polymerase stalls. FANCJ binds to the G4 structure to unwind it and another polymerase is recruited to continue DNA replication.

Fig 3. Map of FANCJ.

The AKKQ sequence (amino acids 129-147) has been highlighted.

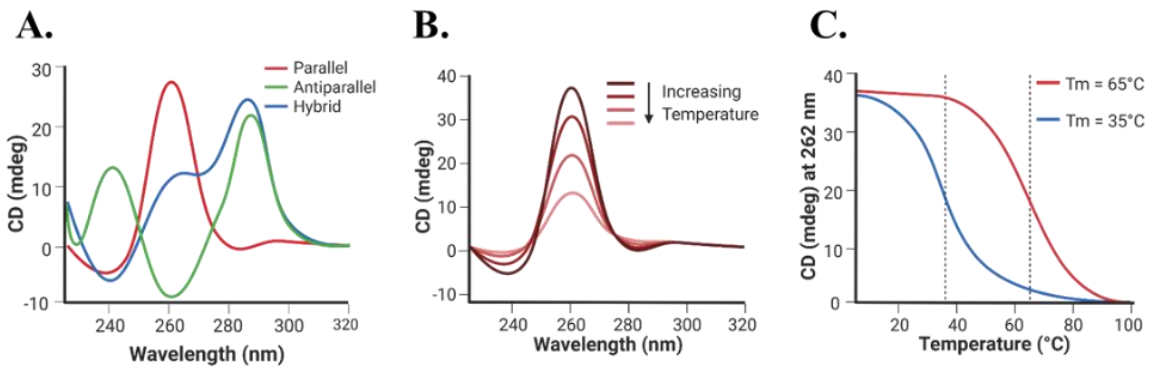

Fig 4. CD spectroscopy cartoons.

(A) Graphic representation of CD spectra for parallel, antiparallel, and hybrid G4 conformations. Parallel conformations have a maximum at 262 nm and a minimum at 240 nm. Antiparallel conformations give two peak signals near 295 nm and 240 nm, and a minimum at 260 nm. Hybrid conformations show a peak at 295 nm, a shoulder around 260 nm, and a minimum at 240 nm. (B) Graphic representation of the CD spectra of a parallel G4 conformation as a function of temperature. (C) Graphic representation of a thermal melt graph of two G4s.

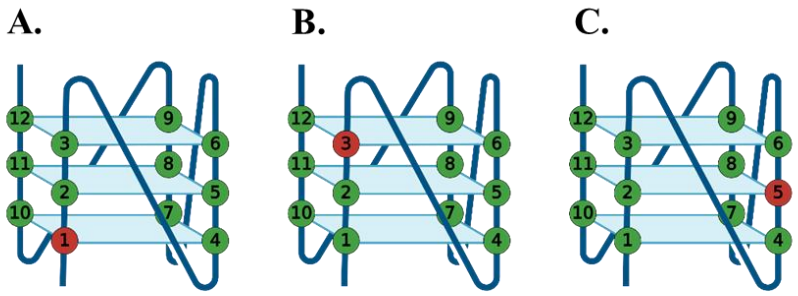

Fig 5. Graphic representation of a parallel G4 conformation.

An 8oxoG-modified base has been substituted at the (A) first guanine (8oxo1), (B) third guanine (8oxo3), and (C) fifth guanine (8oxo5).

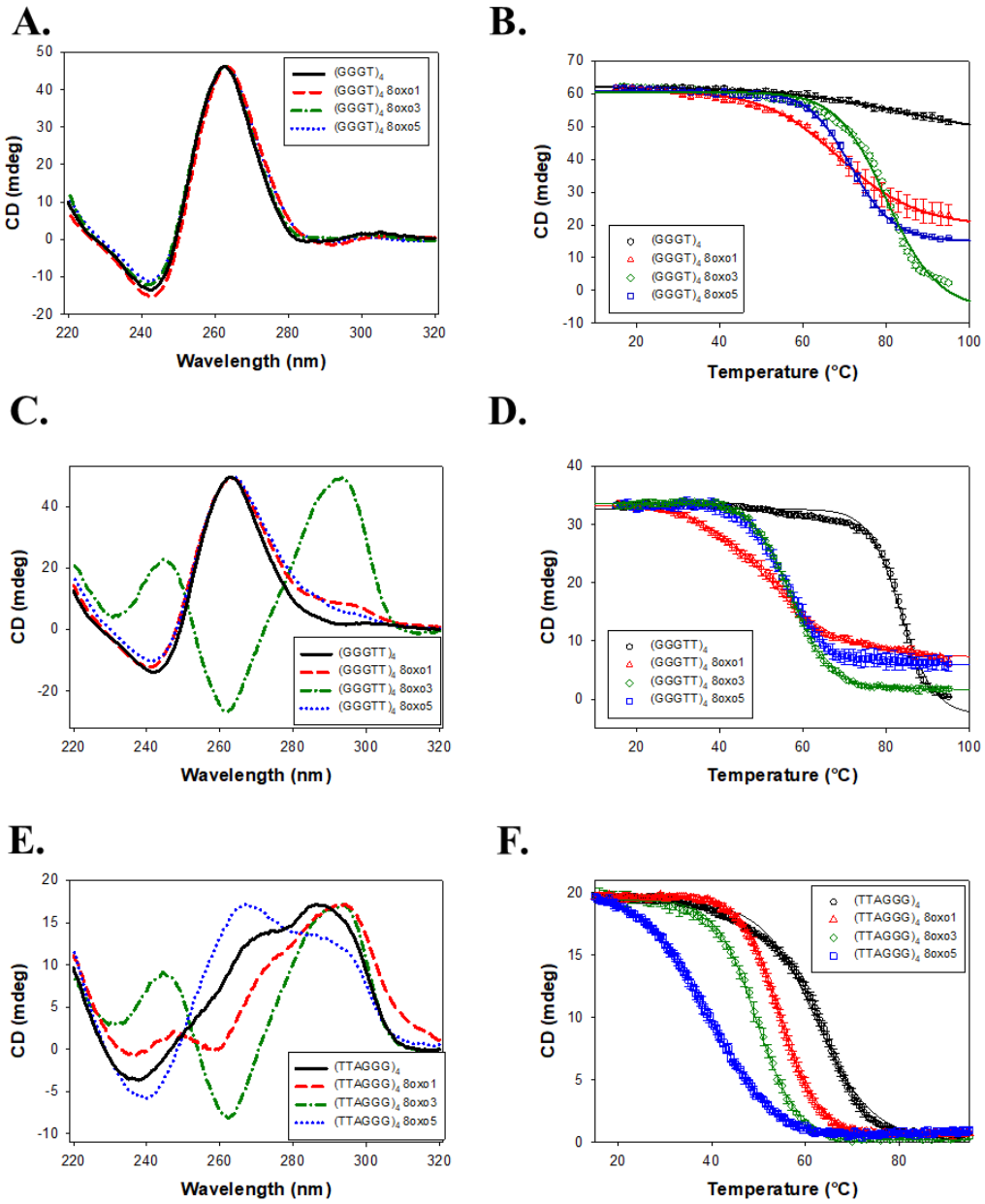

Fig 6. Experiments performed in the presence of 150 mM KCl.

(A) CD spectra of $(GGGT)_4$, $(GGGT)_4$ 8oxo1, $(GGGT)_4$ 8oxo3, and $(GGGT)_4$ 8oxo5 taken from 320 to 220 nm. (B) Temperature melt of same sequences seen in 6A. Melt taken at 262 nm from 15 to 95 °C. (C) CD spectra of $(GGGTT)_4$, $(GGGTT)_4$ 8oxo1, $(GGGTT)_4$ 8oxo3, and $(GGGTT)_4$ 8oxo5 taken

545 from 320 to 220 nm. (D) Temperature melt of same sequences seen in 6C.
546 Melt taken at 262 nm for all sequences except $(GGGTT)_4$ 8oxo3, which was
547 taken at 295 nm. (E) CD spectra of $(TTAGGG)_4$, $(TTAGGG)_4$ 8oxo1,
548 $(TTAGGG)_4$ 8oxo3, and $(TTAGGG)_4$ 8oxo5 taken from 320 to 220 nm. (F)
549 Temperature melt of the same sequences seen in 6E. Melt taken at 295 nm.

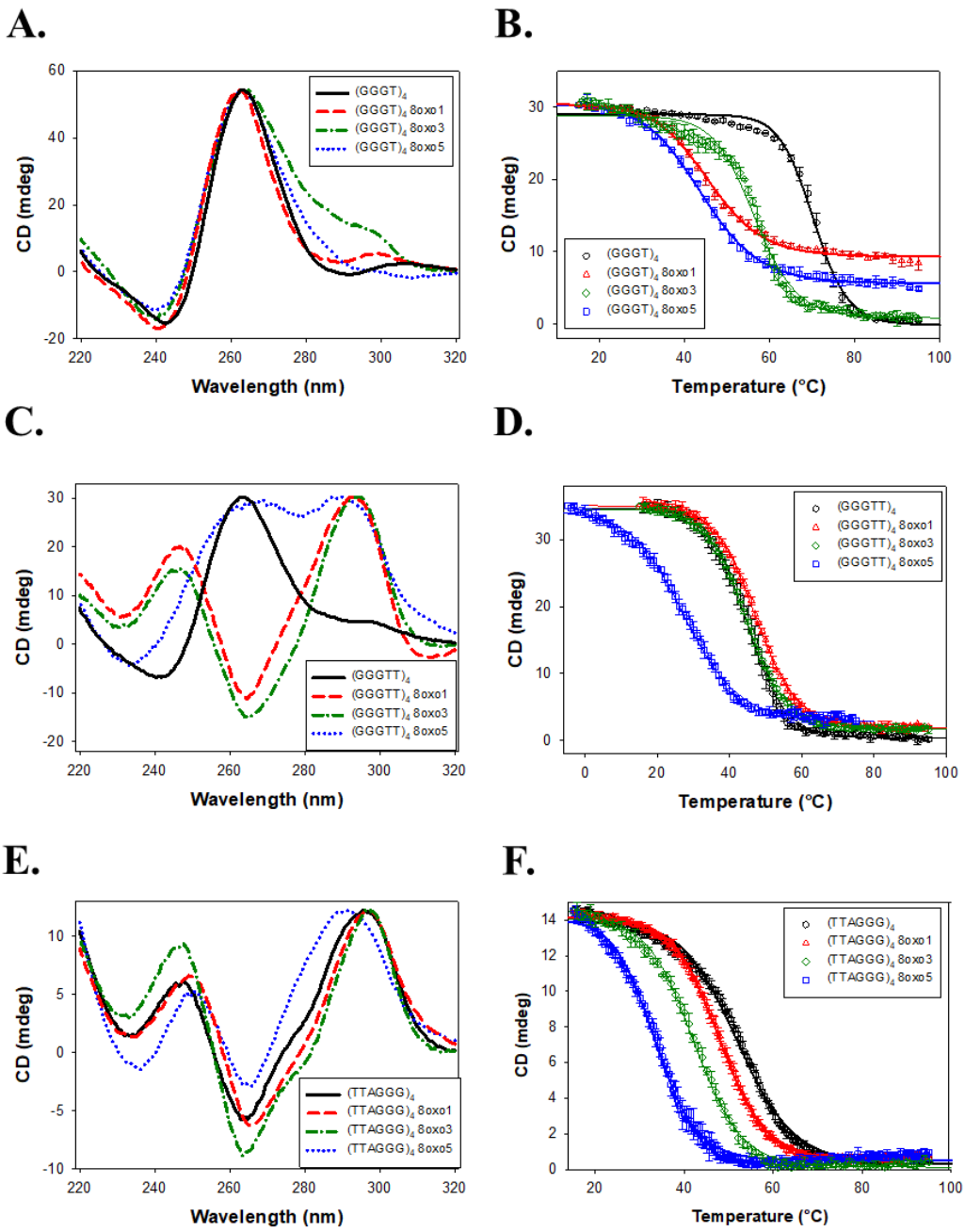

Fig 7. Experiments performed in the presence of 150 mM NaCl.

(A) CD spectra of $(GGGT)_4$, $(GGGT)_4$ 8oxo1, $(GGGT)_4$ 8oxo3, and $(GGGT)_4$ 8oxo5 taken from 320 to 220 nm. (B) Temperature melt of same sequences as seen in 7A. Melt taken at 262 nm from 15 to 95 °C. (C) CD spectra of

555 $(GGGTT)_4$, $(GGGTT)_4$ 8oxo1, $(GGGTT)_4$ 8oxo3, and $(GGGTT)_4$ 8oxo5 taken
556 from 320 to 220 nm. (D) Temperature melt of same sequences as seen in 7C.
557 Melt taken at 262 nm for all sequences except $(GGGTT)_4$ 8oxo3, which was
558 taken at 295 nm. (E) CD spectra of $(TTAGGG)_4$, $(TTAGGG)_4$ 8oxo1,
559 $(TTAGGG)_4$ 8oxo3, and $(TTAGGG)_4$ 8oxo5 taken from 320 to 220 nm. (F)
560 Temperature melt of the same sequences as seen in 7E. Melt taken at 295
561 nm.

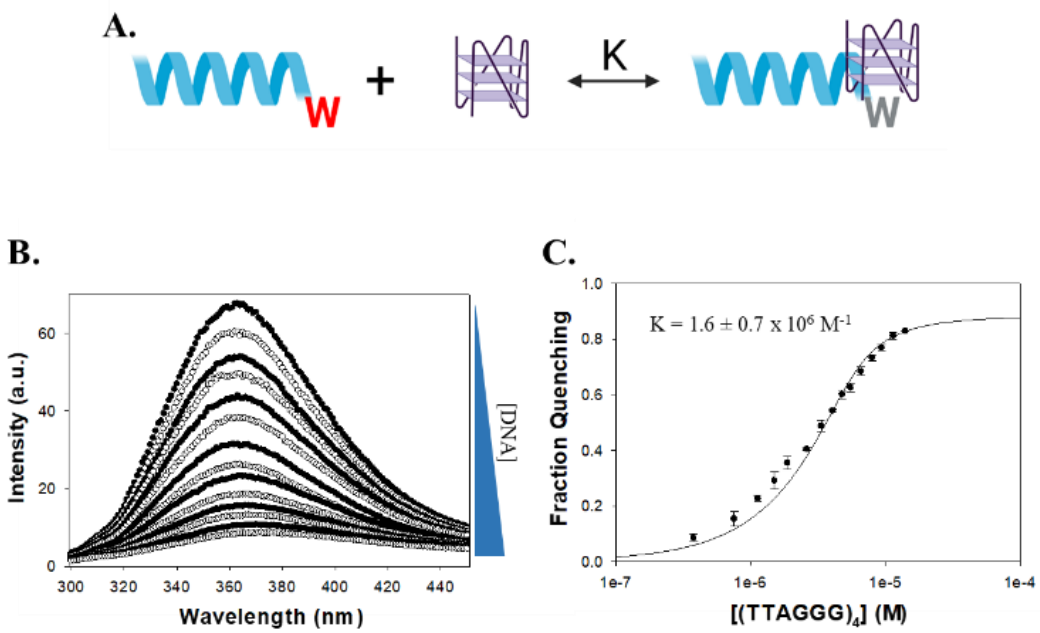

Fig 8. Overview of fluorescence spectroscopy analyses.

(A) Molecular model of fluorescence spectroscopy titrations. AKKQ is equipped with a tryptophan residue that fluoresces. When bound to DNA, the residue is quenched and fluorescence intensity decreases. (B) Titration of AKKQ with $(GGGT)_4$. As DNA concentration increases, the peak intensity decreases. (C) Analysis of fluorescence titration. The decrease in integrated peak is plotted as a function of DNA concentration. The resulting isotherm is fit to a 1:1 binding interaction model to generate an equilibrium K value.

572

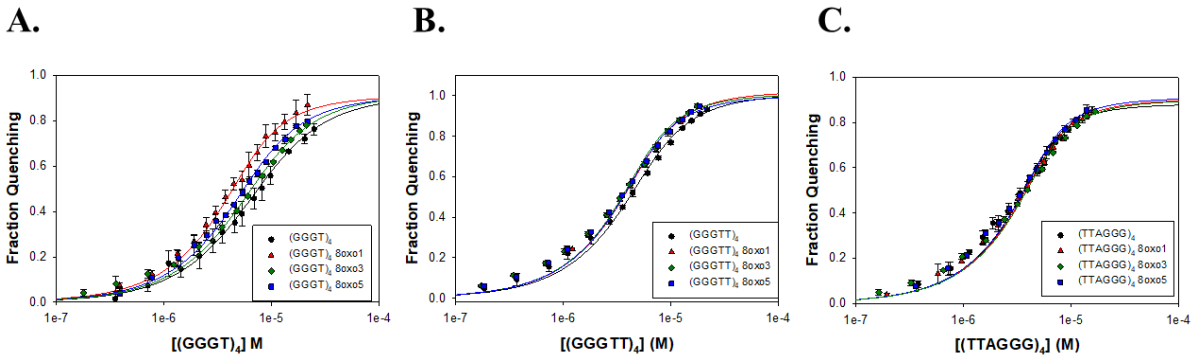

573 **Fig 9. Summary of FANCJ AKKQ-G4 binding in KCl by fluorescence**

574 **spectroscopy.**

575 Trials performed in 20 mM HEPES pH 7.5, 150 mM KCl, 5 mM TCEP, and

576 5% (v/v) glycerol. (A) FANCJ AKKQ equilibrium binding to $(GGGT)_4$ and

577 its respective 8oxoG4 sequences. (B) FANCJ AKKQ binding to $(GGGTT)_4$

578 and its respective 8oxoG4 sequences. (C) FANCJ AKKQ binding to

579 $(TTAGGG)_4$ and its respective 8oxoG4 sequences.

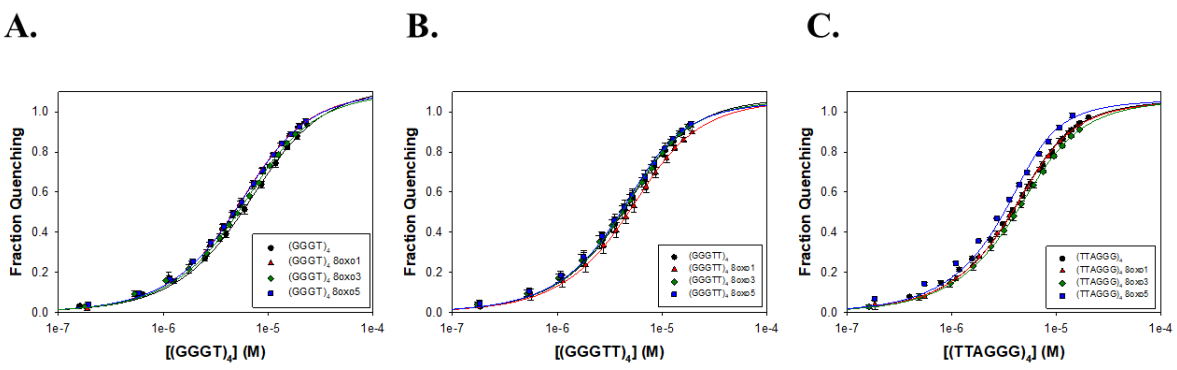

Fig 10. Summary of FANCJ AKKQ-G4 binding in NaCl by fluorescence spectroscopy.

Trials performed in 20 mM HEPES pH 7.5, 150 mM NaCl, 5 mM TCEP, and 5% (v/v) glycerol. (A) FANCJ AKKQ binding to $(GGGT)_4$ and respective 8oxoG4 sequences. (B) FANCJ AKKQ binding to $(GGGTT)_4$ and respective 8oxoG4 sequences. (C) FANCJ AKKQ binding to $(TTAGGG)_4$ and respective 8oxoG4 sequences.

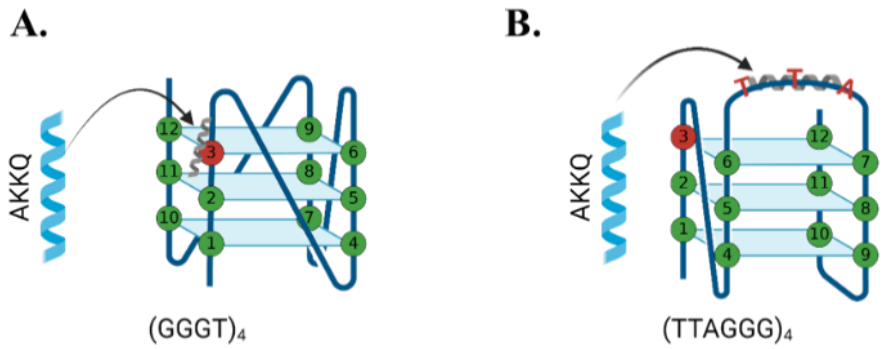

588

589 **Fig 11. Proposed binding interaction model between FANCJ AKKQ and**

590 **8oxoG4 sequences.**

591 (A) For G4 sequences that form compact structures with short intervening

592 sequences, such as $(GGGT)_4$, AKKQ preferentially targets the 8oxoG site

593 and promotes repair. (B) For G4 sequences that expose the intervening

594 sequence, as with antiparallel or hybrid conformations, AKKQ

595 preferentially targets the intervening sequence and ignores the 8oxoG.